NIH Public Access
Author Manuscript
Appl Immunohistochem Mol Morphol. Author manuscript; available in PMC 2007 September 24.

Published in final edited form as:
Appl Immunohistochem Mol Morphol. 2007 March ; 15(1): 113–119.

Comparing Vasculogenic Mimicry with Endothelial Cell Lined Vessels: Techniques for 3D Reconstruction and Quantitative Analysis of Tissue Components from Archival Paraffin Blocks

Amy Y. Lin, MD[*], **Zhuming Ai, PhD**[†], **Sang-Chul Lee, PhD**[‡], **Peter Bajcsy, PhD**[‡], **Jacob Pe'er, MD**[§], **Lu Leach, BS**[*], **Andrew J. Maniotis, PhD**[*], and **Robert Folberg, MD**[*]

*****From the Department of Pathology, University of Illinois at Chicago, Chicago, IL

†From the Department of Biomedical and Health Information Sciences, University of Illinois at Chicago, Chicago, IL

‡From the National Center for Supercomputing Applications, University of Illinois at Urbana-Champaign, Champaign, IL

§From the Department of Ophthalmology, Hadassah-Hebrew University Medical Center, Jerusalem, Israel

Abstract

We previously described techniques to generate 3D reconstructions of the tumor microcirculation using immunofluorescence histochemistry and laser scanning confocal microscopy on serial sections from archival formalin-fixed, paraffin embedded tissues. By aligning sequential z-stacks in an immersive visualization environment (ImmersaDesk), the need to insert fiduciary markers into tissue was eliminated. In this study, we developed methods to stitch overlapping confocal z-series together to extend the surface area of interest well beyond that captured by the confocal microscope objective and developed methods to quantify the distribution of markers of interest in three dimensions. These techniques were applied to the problem of comparing the surface area of non-endothelial cell lined, laminin-rich looping vasculogenic mimicry (VM) patterns, that are known to transmit fluid, with the surface area of endothelial cell lined vessels in metastatic uveal melanoma to the liver in three dimensions. After labeling sections with antibodies to CD34 and laminin, the surface area of VM patterns to vessels was calculated by segmenting out structures that labeled with laminin but not with CD34 from those structures labeling with CD34, or CD34 and laminin. In metastatic uveal melanoma tissues featuring co-localization of high microvascular density [66.4 microvessels adjusted for 0.313 mm^2 area (range 56.7-72.7)] and vasculogenic mimicry patterning, the surface area of vasculogenic mimicry patterns was 11.6 fold greater (range 10.8-14.1) than the surface provided by CD34-positive vessels. These methods may be extended to visualize and quantify molecular markers in three dimensions in a variety of pathological entities from archival paraffin embedded tissues.

Keywords

laser scanning confocal microscopy; immunohistochemistry; 3D reconstruction; melanoma; vasculogenic mimicry

Corresponding Author: Robert Folberg, Department of Pathology, University of Illinois at Chicago, 1819 W. Polk Street (446 CMW), Chicago, Illinois 60612; phone – 312.996.4601; fax – 312 996.7486; e-mail rfolberg@uic.edu

Supported by National Eye Institute Grant EY10457 and Core Grant EY10792

NIH-PA Author Manuscript
NIH-PA Author Manuscript
NIH-PA Author Manuscript

NIH-PA Author Manuscript

NIH-PA Author Manuscript

NIH-PA Author Manuscript

Introduction

Although pathologists render diagnoses based on two-dimensional (2D) histological sections, considerable information about the biology of disease processes resides in the appearance of features in interest in three dimensions (3D). For example, at least two different components of the tumor microcirculation have been shown to have prognostic significance when examined from 2D histological sections: microvascular density (MVD)[1] and looping vasculogenic mimicry (VM) patterns.[2] VM patterns are generated by highly invasive tumor cells and therefore do not label with endothelial cell markers.[3] Because VM patterns connect to blood vessels[4-7] and provide for the circulation of fluid in tumor tissues,[3, 5, 6, 8] the patterns have been called the “fluid-conducting meshwork”.[8, 9]

There is considerable confusion in the literature about the 3D configuration of VM pattering.[10] It has been suggested that the 2D appearance of VM patterns as loops is generated by histological sections taken through tumor spheroids wrapped by extracellular matrix.[10] Investigating the 3D configuration of VM patterns in human tissues became a research priority because these patterns conduct fluid outside of the endothelial cell lined vascular system,[3, 6-9] and therefore might provide a greater surface area for the delivery of therapeutic agents than vessels alone.

A comparison between the 3D configuration of blood vessels and VM patterns was undertaken in paraffin-embedded tissues. Although the application of immunohistochemistry to thick frozen sections would allow for the 3D reconstruction and eliminate artifacts introduced by paraffin embedding,[11] VM patterns are not distributed homogeneously through melanoma tissue,[12] and banked frozen tissue may not contain VM patterns for 3D reconstruction. In 1994, Rummelt et al[13] reconstructed tumor blood vessels in histologic sections of melanoma by laser scanning confocal microscopy (LSCM) from a single, thick, paraffin-embedded tissue sample. Although this method eliminated concern about heterogeneous distortions in paraffin-embedded tissue from section to section when serial sections are used for reconstruction, the penetration of antibodies into very thick paraffin-embedded tumor section was uneven, making it difficult to discriminate between the absence of a signal and a lack of complete penetration of the antibody of interest.

In 2003, Chen et al[7] designed a novel approach to tissue reconstruction on archival paraffin-embedded tissue by combining LSCM on serial tissue sections with reconstruction in an immersive stereo 3-D environment[14] that had been used to visualize molecules and their receptors interactively.[15] With this approach, confocal z-stacks for each serial paraffin section were aligned in the reconstruction process such that information contained within the paraffin section contributes to the reconstruction. With this approach, it was not necessary to insert fiduciary markers that can distort tissue in the area of interest, and it is possible to correct for alignment and tissue distortions by applying warping algorithms on volumetric serial sections. These techniques were used to reconstruct normal vessels in tonsillar tissue and tumors from archival paraffin blocks, and the prognostically significant back-to-back loop configuration of VM patterns in 2D histological sections was shown to represent cross sections through cylindrical (not spherical) sleeves of laminin-rich extracellular matrix surrounding branching cylindrical projections of tumor cells.[7] This analysis, however, was limited to a very small surface area of tissue (captured by a 20X objective in the confocal microscope) and did not include a comparison of the 3D surface areas of endothelial cell lined vessels and non-endothelial cell lined VM patterns.

In the current study, we extended the technological methods of Chen et al[7] to study areas of interest in each tissue section larger than that captured by the objective of the LCSM by automated tiling of overlapping LSCM z-series of each section. We next aligned these large-

NIH-PA Author Manuscript

NIH-PA Author Manuscript

NIH-PA Author Manuscript

area confocal z-series using the immersive visualization environment[7] to generate a 3D reconstruction of tissue. Because VM patterns are known to label with laminin and do not label for endothelial cell markers, we were able to compare the surface areas of VM patterns in 3D with the surface areas of CD34-positive blood vessels by applying techniques we developed to segment out (separate) structures labeling with laminin only from structures labeled by CD34, or CD34 plus laminin. Thus, we were able to calculate the relative 3D surface areas of laminin+/CD34− VM patterns to CD34+ vessels (including CD34+/laminin+ and CD34+/laminin− vessels). Although these techniques were applied to the specific problem of understanding the 3D morphology of VM patterning relative to vessels, these strategies can be applied to other morphological problems that require 3D analysis of marker expression archival tissues in paraffin.

MATERIALS AND METHODS

Experimental strategy and tissue selection

Uveal melanoma tissue – both primary and metastatic – tends to lack stromal elements except for VM patterning. VM patterning, generated by the tumor cell and not a component of the host response, can be distinguished from fibrovascular septa that are seldom encountered in human uveal melanoma tissues that are not necrotic or that have not been treated previously with radiation.[16] By immunohistochemistry, we and others have shown that the cellular elements of these neoplasms are composed almost exclusively of S100-positive tumor cells[17] with secondary populations of macrophages and lymphocytes expressed focally.[18] We and others[7, 19, 20] have demonstrated on two dimensional sections and by 3D reconstructions that zones of high microvascular density tend not co-localize to VM patterns in primary uveal melanoma tissue.

In planning to measure surface areas of VM and tumor vessels in 3D, we reasoned that tumor tissue rich in VM pattering where endothelial cell lined vessels were exceptionally sparse would yield exceptionally high ratios of VM surface area to vascular surface area. We therefore designed this study to determine the lowest ratio of VM pattern surface area to endothelial cell lined vessel surface area by screening more than 40 blocks of primary and metastatic human uveal melanoma tissue for the presence of VM and MVD and we identified regions in hepatic uveal melanoma metastases that featured the unusual co-localization of these two features of interest. The hepatic metastasis tissue had been resected from a patient who was treated for primary uveal melanoma (uveal melanoma tends to disseminate exclusively to the liver as a first site of dissemination[21, 22]). Resected tissue was fixed for 24 hours in 10% neutral buffered formalin before paraffin embedding.

The use of archival human tissue in this study was performed in accordance with the Declaration of Helsinki and was approved by the Institutional Review Board of the University of Illinois at Chicago and the Helsinki Committee at Hadassah-Hebrew University Medical Center.

Immunohistochemistry

Sections were cut at 4 μm thicknesses, floated on a water bath at 42° C for fewer than 5 seconds, mounted on slides, deparaffinized in xylene, and rehydrated through a decreasing ethanol gradient. Heat induced epitope retrieval was accomplished as follows. After hydrating slides in distilled water, slides were exposed for 20 minutes to Dako Target Retrieval Solution (10x concentrate, diluted 10:1; catalog S1699, Dako, Carpinteria, CA) at pH 6.1 that had been heated to 95°C in a vegetable steamer (Oster Vegetable steamer, model 5713, 60 Hz 120 v- 900 watt; Oster, Milwaukee, WI) . Slides were removed from the steamer and allowed to equilibrate to

NIH-PA Author Manuscript

NIH-PA Author Manuscript

NIH-PA Author Manuscript

room temperature for 20 minutes in Target Retrieval Solution, followed by a rinse in distilled water.

For the simultaneous detection of CD34 and laminin in melanoma tissue, slides were incubated with monoclonal mouse anti-human CD34 (QBend10; Dako) at a dilution of 1:40 for 30 minutes and placed in protein-blocking solution (Dako) for 10 minutes. Antibody binding was detected with Alexa Fluor 488 conjugated goat anti-mouse IgG (Invitrogen, Carlsbad, CA) for 30 minutes at a dilution titer of 1:400. After 10 minutes of protein blocking, slides were incubated with polyclonal rabbit anti-laminin antibody (Sigma-Aldrich, St Louis) at a dilution titer of 1:200 for 30 minutes at room temperature. After protein blocking for 10 minutes, antibody binding was detected with Alexa Flour 594-conjugated goat anti-rabbit IgG (Invitrogen) for 30 minutes at a dilution titer of 1:400. Slides were rinsed in buffer and mounted in aqueous mounting medium (Faramount; Dako). For all staining procedures, secondary antibody was omitted in negative control experiments. For the reconstruction of blood vessels and VM patterns, we examined 7 serial sections from each of 4 areas of highly vascularized metastatic uveal melanoma to the liver co-localizing to VM patterns.

Laser scanning confocal microscopy and stitching algorithms

All histologic serial sections were examined with a laser scanning confocal microscope (Leica, Microsystems, Bannockburn, IL) using the 40X objective. Four different areas in the tumor were photographed and images were stored in tagged information file format (TIFF). Each field consisted of a *z*-stack of 13 components obtained at 0.3-μm intervals. Because the size of a 40X field is limited, we captured 9 overlapping fields and stitched these using a fully automated mosaicking algorithm using a standard method for pattern recognition and computer vision. We developed a normalized correlation-based fully automated mosaicking algorithm with standard methods used in pattern recognition and computer vision,[23, 24] so that all possible translational tile overlaps are evaluated based on pixel comparisons according to the Equation (1)

$$E = \frac{\sum_{j=1}^{m}\sum_{i=1}^{n}\left(X(i,\ j) - \mu_X\right)\left(Y(i,\ j) - \mu_Y\right)}{\sqrt{\sum_{j=1}^{m}\sum_{i=1}^{n}\left(X(i,\ j) - \mu_X\right)^2 \sum_{j=1}^{m}\sum_{i=1}^{n}\left(Y(i,\ j) - \mu_Y\right)^2}} \quad (1)$$

where X and Y are images to be compared (adjacent tiles in image mosaicking), and μ is the mean value of the image. The largest correlation coefficient *E* indicates the best match of two tiles and provides the desired translational offset for tile stitching. The main advantages of this method are (a) its relatively low computational cost, (b) robust performance for image tiles acquired with the same instrumentation setup, and (c) full automation.

3D reconstructions

After stitching overlapping areas from each serial section, the z-series from each section were aligned in an immersive 3D environment using ImmersaDesk[14] (Fakespace, Kitchener, Ontario, Canada) by methods described in detail previously.[7, 25] ImmersaDesk[14] is available in image-analysis facilities at many research universities and permits multiple researchers to view data simultaneously, provides investigators with stereo vision, and allows for a wide viewing angle and the ability to present different 3-D aspects of the image depending on the investigator's perspective.

In the immersive environment, the investigator matches alignment of the bottom image of the *z*-series from the first serial section with the top image from the Z-series of the next serial section, while all 3D relationships between the adjacent sections are taken into account in determining the alignment between the sections, repeating this step until all images are aligned

NIH-PA Author Manuscript

NIH-PA Author Manuscript

NIH-PA Author Manuscript

(Fig. 1). If the object of interest in the bottom of the *z*-series of layer 1 does not match the top image in the next layer, the distortion, perhaps introduced by tissue processing, is corrected by applying a 3-D nonlinear warping algorithm restore the distortion after the initial manual alignment. We use automated image reconstruction (AIR) software to apply a 2-D non-linear warping algorithm to match the bottom image of the *z*-series from layer 1 with the top image from the *z*-series of layer 2, resulting in a 2-D *n*th order polynomial transformation which is expanded to 3-D (*n* +1)th order as described in detail elsewhere.[25] With the known boundary conditions and some reasonable assumptions, all the coefficients in the *(n* + 1)th-order polynomial can be determined, and with this nonlinear transformation, the z-series from adjacent serial sections can be warped to connect to each other smoothly. The size of each reconstructed volume was restrained to less than 512 × 512 × 256 voxels to accommodate software and hardware limitations.

Segmentation and Calculation of Surface Areas

In this study, laminin was labeled red and CD34-positive endothelial cells were labeled green. Non endothelial cell lined laminin-rich VM patterns were segmented (isolated for analysis) by removing green (CD34+ endothelium) and yellow (co-localization of CD34+ endothelial cells and laminin) voxels from the volume, and converting the RGB volume to a gray scale volume:

$$I_{xyz} = \begin{cases} R_{xyz}, & if\ G_{xyz} = 0 \\ 0, & if\ G_{xyz} > 0 \end{cases},$$

where R_{xzy} and G_{xzy} are red and green component of the RGB volume at position (*x*, *y*, *z*) respectively, and I_{xyz} is the intensity of the converted gray scale volume at (*x*, *y*, *z*). Blood vessels (appearing either green or yellow) were segmented (isolated for analysis) by removing red voxels (representing laminin not associated with endothelium) from the volume: $I_{xyz}=G_{xyz}$.

After the segmented laminin and blood vessels were converted to gray scale volumes, the marching cubes algorithm[26] was used to convert the volumetric model to a surface model, and the surface areas of laminin in VM patterns and endothelial cell lined blood vessels were calculated using the Visualization Tool Kit (VTK).[27] A threshold is needed in the marching cubes algorithm to determine where the surfaces of laminin and blood vessels are. To maintain consistency in calculations, the threshold value of 64 was used in the marching cubes algorithm in all the studies.

Microvascular Density

Microvascular density was determined by counting the number discreet CD34+ labeling points from an *en face* (two-dimensional) projection of each reconstruction. Even in highly vascularized primary and metastatic uveal melanoma tissues, the distribution of blood vessels within vasculogenic mimicry patterns is uneven. We therefore restricted the area of interest to allow for the examination of tumor tissue with the highest concentration of blood vessels within vasculogenic mimicry patterns. There are limitations to the size of volumetric data that can be analyzed in the ImmersaDesk environment. We therefore quantified the 3D surface areas of VM patterns and vessels where the number of vessels was highest, but the surface area for any plane within this volumetric construction was less than 0.313 mm^2. To allow for a comparison between our data and data reported in the literature, we calculated an adjusted MVD for the conventional area used for reporting this parameter (Table 1): the MVD in areas of tissue examined in this study is in the high range of MVD measurements in this tumor system.[19, 20]

NIH-PA Author Manuscript

NIH-PA Author Manuscript

NIH-PA Author Manuscript

RESULTS

The liver metastasis from uveal melanoma contained numerous back-to-back laminin+ VM loops (Fig. 2), as well as numerous small blood vessels (Fig. 3). When measured from a 2D histological section adjusted for an area of 0.313 mm^2, the microvascular density in all samples was high using the criteria reported by Makitie et al[19] for this primary uveal melanoma (range 56.7-72.7 vessels/0.313 mm^2, Table 1). When measured from the 3D reconstructed tissue, the average ratio of the surface area of looping CD34−/laminin+ VM patterns to the surface area of CD34+ blood vessels was 11.6 (range 10.8-14.1, Table 1).

DISCUSSION

It is possible to derive information about the structure of tissue elements in 3D that would not necessarily be anticipated from the examination of 2D histological sections. Specifically, using 3D reconstructions, we demonstrated that the histological finding of back-to-back loops (VM patterning) in melanoma tissue represents cross sections of cylindrical structures rather than spheroids as originally postulated.[7] The finding is clinically relevant because VM patterns transmit fluid in tissue and may be a conduit for drug delivery.[6, 8, 9] The distribution of fluid around cylinders is clearly different from the distribution around spheroids.

In our previous and current work, tissues were reconstructed from confocal stacks generated from serial paraffin sections. One may reasonably question why is it necessary to account for histological features contained within the thickness of the section: why shouldn't the reconstruction to be performed from measuring surface areas on adjacent serial sections, eliminating the need for confocal microscopy? There are at least two significant limitations to the reconstruction of tissue without considering the depth of the structure in tissue sections. First, the volumetric content of the confocal stack permits serial sections to be aligned correctly (Figure 1).[7, 25] The currently available alternative to volumetric-assisted construction requires the insertion of fiduciary markers into tissue that may distort the tissue. Second, if one reconstructs tissue without considering the information contained within the thickness of each serial section, then information (resolution) is lost: the thicker the section used for reconstruction purposes, the more information that is lost.

Investigators who plan to reconstruct tissue using the technique of aligning volumetric stacks in an immersive visualization environment may consider using serial sections that are thicker than the 4 μm sections used in this study. Fewer serial thick sections are required to reach the same volumetric construction as reconstructions of thinner sections. We experimented with tissue sections of varying thicknesses. For example, in our hands, we found that there was excellent antibody penetration at 10 μm, but that it was more difficult to capture sequential artifact-free sections at this thickness. As sections increased in thickness, the number of artifacts increased as well. A fold or distortion in one of several adjacent sections will interfere with the reconstruction. In our laboratory, the most efficient throughput for adjacent artifact-free serial sections was achieved at 4 μm thickness, but we acknowledge that other laboratories may be capable of generating reconstructions from thicker serial sections.

In our previous work[7, 25] and in this study, we selected a manual method to align volumetric confocal data with the of confocal stacks using the ImmersaDesk visualization environment. It is now possible to port much of the functionality of the ImmersaDesk to individual computer workstations (unpublished data). We are also developing semi-automated and automated alignment tools that yield results comparable to those achieved by manual methods[28] and do not require the insertion of fiduciary markers that can distort tissue.

In this study, we introduced two new methods to our 3D reconstruction strategies. First, we developed a method to stitch together the z-stacks of overlapping confocal fields of interest.

NIH-PA Author Manuscript

NIH-PA Author Manuscript

NIH-PA Author Manuscript

This permitted us to extend the reconstruction field of view in the x and y axes beyond the area captured by the confocal microscope objective. Second, we developed a method to measure the surface area of the objects of interest (blood vessels and VM patterns) in 3D. We then applied these methods to the problem of comparing the surface areas of blood vessels with VM patterning. Because a high concentration of blood vessels seldom co-localizes to VM patterning in primary uveal melanomas, we studied foci of metastatic uveal melanoma to the liver where such co-localization was identified.

For this study, we selected CD34 (QBend 10) to label blood vessel endothelium because this marker does not label the endothelium of hepatic sinusoids (in normal liver, CD34 expression is confined to periportal vessels)[29] and has been shown previously to generate the highest MVD calculations in this tumor system among multiple endothelial cell labels tested.[19] As noted above, tissue from which the reconstruction was generated did not contain stromal elements other than VM patterns. We have previously described CD34 labeling of melanoma cells,[20] but these inappropriately labeled tumor cells can be identified in three dimensional reconstructions because they appear rounded (when CD34 labels melanoma cells, the tumor cells are typically epithelioid, not spindled)[20] and multiple cells stain in grapelike clusters.[7] In the reconstruction performed in this study, we confirmed that CD34-positive elements formed tubular structures consistent with vessels by rotating the reconstructed image to visualize the areas of interest from multiple points of view.

It is certainly possible to use alternative labels for blood vessel endothelium such as CD31 or CD105, or to employ multiple endothelial cell labels simultaneously to study the 3D distribution of blood vessel endothelial cells expressing different markers. It is also feasible to extend these observations to the study of additional structures of interest, such as the relative distribution of lymphatics within the hepatic metastases by introducing a third label to lymphatic endothelium such as podoplanin or D2-40.[30] Segmentation of the third channel by methods similar to those described above would permit us to isolate the surface area of lymphatic vessels in the hepatic metastasis (there are no lymphatic channels within primary uveal melanomas[31]).

VM patterns are generated by highly invasive tumor cells and do not label with endothelial cell markers. Looping vasculogenic mimicry (VM) patterns were first described as a histological marker of adverse outcome in uveal melanomas[19, 32-36] and were identified in hepatic melanoma metastases[37] using the non-specific modified periodic acid-Schiff stain.[38] VM patterns are now known to contain laminin,[9, 20] fibronectin,[39] collagen IV,[40] collagen VI,[41] and focal trace amounts of collagen I[39] and to be different from fibrovascular septa in both composition and morphology.[16] Aside from uveal melanomas, VM patterns have been demonstrated histologically in cutaneous[42, 43] and oral mucosal melanomas,[44] inflammatory[45-50] and ductal[51] breast carcinoma, and prostatic carcinoma,[52] ovarian carcinoma,[53] rhabdomyosarcoma[40] and synoviosarcoma,[54] and pheochromocytoma.[55]

In areas of tumor tissue where high MVD co-localize to VM pattens, the laminin-positive CD34-negative VM patterns provide for an 11.6 fold greater (range 10.8-14.1) surface area than CD34-positive blood vessels. In most primary tumors, where blood vessels seldom co-localize to zones of high MVD, it is likely that the ratio of VM surface area to the surface area of endothelial cell-lined blood vessels is much greater. Therefore, the potential surface afforded by VM patterns may provide an augmented distribution of therapeutic compounds to tumor tissue beyond that provided by blood vessels alone.

Without the application of 3D reconstruction techniques following immunohistochemistry and confocal microscopy, it would not have been possible to clarify the spatial configuration of VM patterns or to quantify the relative surface areas of endothelial cell lined blood vessels to

NIH-PA Author Manuscript

NIH-PA Author Manuscript

NIH-PA Author Manuscript

these patterns. The techniques used in this study illustrate the convergence of immunohistochemistry and macroscopic 3D tissue reconstruction. The ability to apply these techniques to archival paraffin blocks may make it possible for pathologists to visualize and quantify the distribution of molecular markers in a variety of tissues and pathological entities in 3D.

References

1. Weidner N. Tumoral vascularity as a prognostic factor in cancer patients - the evidence continues to grow. J Pathol 1998;184:119–122. [PubMed: 9602700]
2. Folberg R, Maniotis AJ. Vasculogenic mimicry. APMIS 2004;112:508–525. [PubMed: 15563313]
3. Maniotis AJ, Folberg R, Hess A, et al. Vascular channel formation by human melanoma cells in vivo and in vitro: vasculogenic mimicry. Am J Pathol 1999;155:739–752. [PubMed: 10487832]
4. Folberg R, Mehaffey M, Gardner LM, et al. The microcirculation of choroidal and ciliary body melanomas. Eye 1997;11:227–238. [PubMed: 9349418]
5. Folberg R, Hendrix MJ, Maniotis AJ. Vasculogenic mimicry and tumor angiogenesis. Am J Pathol 2000;156:361–381. [PubMed: 10666364]
6. Maniotis AJ, Chen X, Garcia C, et al. Control of melanoma morphogenesis, endothelial survival, and perfusion by extracellular matrix. Lab Invest 2002;82:1031–1043. [PubMed: 12177242]
7. Chen X, Ai Z, Rasmussen M, et al. Three-dimensional reconstruction of extravascular matrix patterns and blood vessels in human uveal melanoma tissue: techniques and preliminary findings. Invest Ophthalmol Vis Sci 2003;44:2834–2840. [PubMed: 12824220]
8. Clarijs R, van Dijk M, Ruiter DJ, et al. Functional and morphologic analysis of the fluid-conducting meshwork in xenografted cutaneous and primary uveal melanoma. Invest Ophthalmol Vis Sci 2005;46:3013–3020. [PubMed: 16123395]
9. Clarijs R, Otte-Holler I, Ruiter DJ, et al. Presence of a fluid-conducting meshwork in xenografted cutaneous and primary human uveal melanoma. Invest OphthalmolVisSci 2002;43:912–918.
10. McDonald DM, Munn L, Jain RK. Vasculogenic mimicry: how convincing, how novel, and how significant? Am J Pathol 2000;156:383–388. [PubMed: 10666365]
11. Brey EM, King TW, Johnston C, et al. A technique for quantitative three-dimensional analysis of microvascular structure. Microvasc Res 2002;63:279–294. [PubMed: 11969305]
12. Folberg R, Fleck M, Mehaffey MG, et al. Mapping prognostically significant vascular patterns in ciliary body and choroidal melanomas. Pathol Oncol Res 1996;2:229–236. [PubMed: 11173608]
13. Rummelt V, Gardner LM, Folberg R, et al. Three-dimensional relationships between tumor cells and microcirculation using double cyanine-immunolabeling, laser scanning confocal microscopy and computer-assisted reconstruction: an alternative to cast corrosion preparations. J Histochem Cytochem 1994;42:681–686. [PubMed: 7908912]
14. Czernuszenko M, Pape D, Sandin D, et al. The ImmersaDesk and infinity wall projection-based virtual reality displays. Comp Graphics 1997;31:46–49.
15. Nagata H, Mizushima H, Tanaka H. Concept and prototype of protein-ligand docking simulator with force feedback technology. Bioinformatics 2002;18:140–146. [PubMed: 11836222]
16. Lin AY, Maniotis AJ, Valyi-Nagy K, et al. Distinguishing fibrovascular septa from vasculogenic mimicry patterns. Arch Pathol Lab Med 2005;129:884–892. [PubMed: 15974811]
17. Chen YF, Chiu HH, Wu CH, et al. Retinoblastoma protein (pRB) was significantly phosphorylated through a Ras-to-MAPK pathway in mutant K-ras stably transfected human adrenocortical cells. DNA Cell Biol 2003;22:657–664. [PubMed: 14611687]
18. Makitie T, Summanen P, Tarkkanen A, et al. Tumor-infiltrating macrophages (CD68(+) cells) and. prognosis in malignant uveal melanoma. Invest Ophthalmol Vis Sci 2001;42:1414–1421. [PubMed: 11381040]
19. Makitie T, Summanen P, Tarkkanen A, et al. Microvascular density in predicting survival of patients with choroidal and ciliary body melanoma. Invest Ophthalmol Vis Sci 1999;40:2471–2480. [PubMed: 10509639]

NIH-PA Author Manuscript

NIH-PA Author Manuscript

NIH-PA Author Manuscript

20. Chen X, Maniotis AJ, Majumdar D, et al. Uveal melanoma cell staining for CD34 and assessment of tumor vascularity. InvestOphthalmolVisual Sci 2002;43:2533–2539.
21. Lorigan JG, Wallace S, Mavligit GM. The prevalence and location of metastases from ocular melanoma: imaging study in 110 patients. Am J Radiol 1991;157:1279–1281.
22. Albert DM, Ryan LM, Borden EC. Metastatic ocular and cutaneous melanoma: A comparison of patient characteristics and prognosis. Arch Ophthalmol 1996;114:107–108. [PubMed: 8540843]
23. Pratt WK. Correlation techniques for image resolution. IEEE Aerospace Elect Syst 1974;10:353–358.
24. Duda, R.; Hart, P.; Stork, D. Wiley-Interscience; New York, NY: 2001. Pattern Classification; p. 654Edited by
25. Ai ZM, Chen X, Rasmussen M, et al. Reconstruction and exploration of three-dimensional confocal microscopy data in an immersive virtual environment. Comput Med Imaging Graph 2005;29:313–318. [PubMed: 15893451]
26. Lorensen W, Cline H. Marching cubes: A high resolution 3D surface construction algorithm. Comp Graph 1987;21:163–169.
27. Schroeder, W.; Martin, K.; Lorensen, W. Prentice Hall; Upper Saddle River, NJ: 1996. The Visualization Toolkit: An object-oriented approach to 3D graphics. Edited by
28. Bajcsy P, Lee SC, Lin AY, et al. 3D Volume reconstruction of extracellular matrix proteins in uveal melanoma from fluorescent confocal laser scanning microscope images. J Microsc. 2005
29. Pusztaszeri M, Chaubert P, Seelentag W, et al. Immunohistochemical Expression of Endothelial MARKERS CD31, CD34, von Willebrand Factor, and Fli-1 in Normal Human Tissues. J Histochem Cytochem. 2005
30. Evangelou E, Kyzas PA, Trikalinos TA. Comparison of the diagnostic accuracy of lymphatic endothelium markers: Bayesian approach. Mod Pathol 2005;18:1490–1497. [PubMed: 15990898]
31. Clarijs R, Schalkwijk L, Ruiter DJ, et al. Lack of lymphangiogenesis despite coexpression of VEGF-C and its receptor Flt-4 in uveal melanoma. Investigative Ophthalmology and Visual Sciences 2001;42:1422–1428.
32. Folberg R, Rummelt V, Parys-Van Ginderdeuren R, et al. The prognostic value of tumor blood vessel morphology in primary uveal melanoma. Ophthalmology 1993;100:1389–1398. [PubMed: 8371929]
33. Sakamoto T, Sakamoto M, Yoshikawa H, et al. Histologic findings and prognosis of uveal malignant melanoma in Japanese patients. Am J Ophthalmol 1996;121:276–283. [PubMed: 8597270]
34. McLean IW, Keefe KS, Burnier MN. Uveal melanoma: comparison of the prognostic value of fibrovascular loops, mean of the ten largest nucleoli, cell type and tumor size. Ophthalmology 1997;104:777–780. [PubMed: 9160022]
35. Seregard S, Spangberg B, Juul C, et al. Prognostic accuacy of the mean of the largest nucleoli, vascular patterns, and PC-10 in posterior uveal melanoma. Ophthalmology 1998;105:485–491. [PubMed: 9499780]
36. Makitie T, Summanen P, Tarkannen A, et al. Microvascular loops and networks as prognostic indicators in choroidal and ciliary body melanomas. J Nat Cancer Inst 1999;91:359–367. [PubMed: 10050870]
37. Rummelt V, Mehaffey MG, Campbell RJ, et al. Microcirculation architecture of metastases from primary ciliary body and choroidal melanomas. Am J Ophthalmol 1998;126:303–305. [PubMed: 9727526]
38. Folberg R, Pe'er J, Gruman LM, et al. The morphologic characteristics of tumor blood vessels as a marker of tumor progression in primary human uveal melanoma: a matched case-control study. Hum Pathol 1992;23:1298–1305. [PubMed: 1427757]
39. Lin AY, Maniotis AJ, Valyi-Nagy K, et al. Distinguishing fibrovascular septa from vasculogenic mimicry patterns. Arch Pathol Lab Med 2005;129:884–892. [PubMed: 15974811]
40. Hao XS, Sun BC, Zhang SW, et al. Correlation between the expression of collgen IV, VEGF and vasculogenic mimicry. Zhonghua ZhongLiu Za Zhi 2003;25:524–526.
41. Daniels KJ, Boldt HC, Martin JA, et al. Expression of Type VI collagen in uveal melanoma: role in pattern formation and tumor progression. Lab Invest 1996;75:55–66. [PubMed: 8683940]

NIH-PA Author Manuscript

NIH-PA Author Manuscript

NIH-PA Author Manuscript

42. Thies A, Mangold U, Moll I, et al. PAS-positive loops and networks as a prognostic indicator in cutaneous malignant melanoma. J Pathol 2001;195:537–542. [PubMed: 11745688]
43. Warso MA, Maniotis AJ, Chen X, et al. Prognostic significance of periodic acid-Schiff-positive patterns in primary cutaneous melanoma. Clin Cancer Res 2001;7:473–477. [PubMed: 11297236]
44. Lee YJ, Nagai N, Siar CH, et al. Angioarchitecture of primary oral malignant melanomas. J Histochem Cytochem 2002;50:1555–1562. [PubMed: 12417622]
45. Shirakawa K, Tsuda H, Heike Y, et al. Absence of endothelial cells, central necrosis, and fibrosis are associated with aggressive inflammatory breast cancer. Cancer Res 2001;61:445–451. [PubMed: 11212228]
46. Shirakawa K, Kobayashi H, Heike Y, et al. Hemodynamics in vasculogenic mimicry and angiogenesis of inflammatory breast cancer xenograft. Cancer Res 2002;62:560–566. [PubMed: 11809710]
47. Shirakawa K, Wakasugi H, Heike Y, et al. Vasculogenic mimicry and pseudo-comedo formation in breast cancer. Int J Cancer 2002;99:821–828. [PubMed: 12115483]
48. Kobayashi H, Shirakawa K, Kawamoto S, et al. Rapid accumulation and internalization of radiolabeled herceptin in an inflammatory breast cancer xenograft with vasculogenic mimicry predicted by the contrast-enhanced dynamic MRI with the macromolecular contrast agent G6-(1B4M-Gd)(256). Cancer Res 2002;62:860–866. [PubMed: 11830544]
49. Shirakawa K, Furuhata S, Watanabe I, et al. Induction of vasculogenesis in breast cancer models. Br J Cancer 2002;87:1454–1461. [PubMed: 12454777]
50. Shirakawa K, Kobayashi H, Sobajima J, et al. Inflammatory breast cancer: vasculogenic mimicry and its hemodynamics of an inflammatory breast cancer xenograft model. Breast Cancer Res 2003;5:136–139. [PubMed: 12793894]
51. Buijs JT, Cleton AM, Smit VT, et al. Prognostic significance of periodic acid-Schiff-positive patterns in primary breast cancer and its lymph node metastases. Breast Cancer Res Treat 2004;84:117–130. [PubMed: 14999142]
52. Sharma N, Seftor RE, Seftor EA, et al. Prostatic tumor cell plasticity involves cooperative interactions of distinct phenotypic subpopulations: role in vasculogenic mimicry. Prostate 2002;50:189–201. [PubMed: 11813211]
53. Sood AK, Seftor EA, Fletcher MS, et al. Molecular determinants of ovarian cancer plasticity. Am J Pathol 2001;158:1279–1288. [PubMed: 11290546]
54. Hao X, Sun B, Zhang S, et al. Microarray study of vasculogenic mimicry in bi-directional differentiation malignant tumor. Zhonghua YiXueZa Zhi 2002;82:1298–1302.
55. Favier J, Plouin PF, Corvol P, et al. Angiogenesis and vascular architecture in pheochromocytomas - Distinctive traits in malignant tumors. Am J Pathol 2002;161:1235–1246. [PubMed: 12368197]

NIH-PA Author Manuscript

NIH-PA Author Manuscript

NIH-PA Author Manuscript

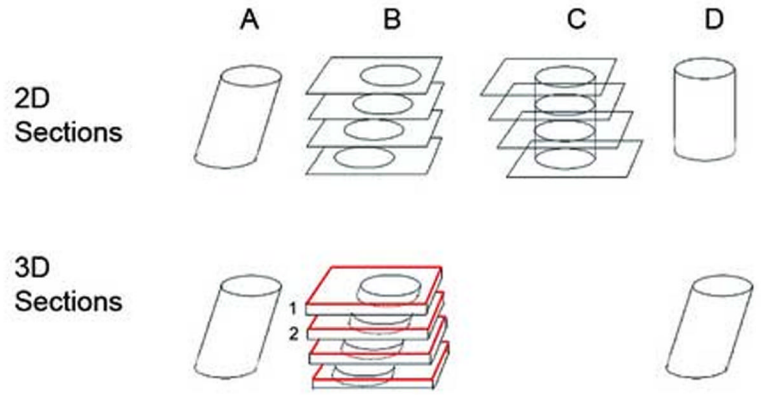

FIGURE 1.

The reconstruction of a tilted cylinder (column A) from 2D sections is illustrated on the top row. One might align cross sections of the cylinder to assemble either the original tilted cylinder (B) or an upright cylinder (C and D). However, if one reconstructs the tilted cylinder from 3D volumetric sections as illustrated on the bottom row, the bottom of the first z-stack (B, layer 1, in black) is aligned with the top image of the 2nd z-stack (B, layer 2, in red) to achieve the alignment that is true to the shape of the original object in the final reconstruction (D). The process is repeated on the z-stacks of adjacent sections (bottom of one stack to the top of the adjacent stack). Sections are shown in this sketch as separated in space only for the purposes of illustration.

NIH-PA Author Manuscript

NIH-PA Author Manuscript

NIH-PA Author Manuscript

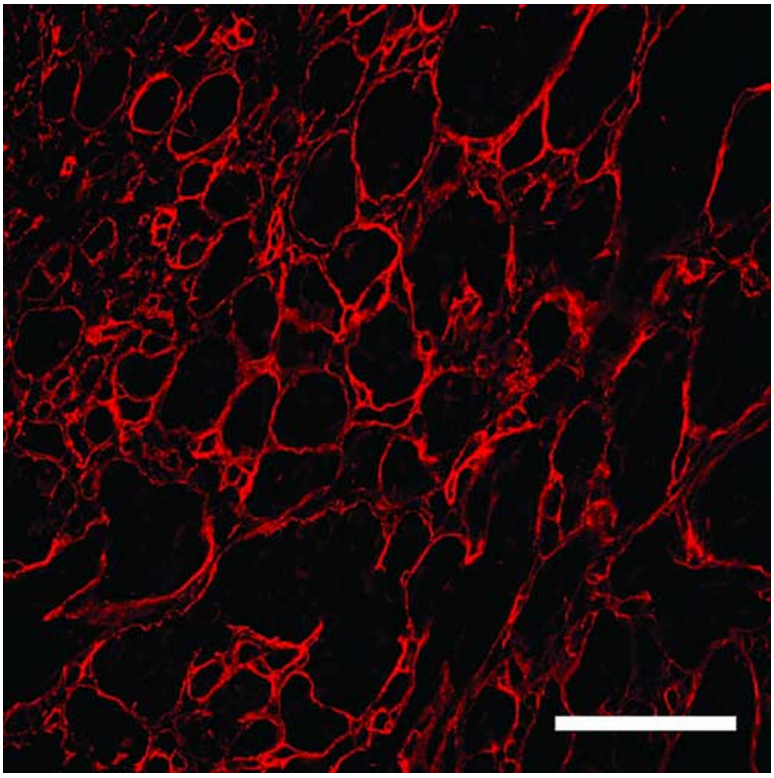

FIGURE 2.

Back-to-back loops of laminin, characteristic of vasculogenic mimicry patterns are illustrated in one 2D plane from the reconstruction of area 4 (see Fig. 3 for the complete reconstruction of this tissue). The green channel (staining for CD34) is subtracted from this image but is included in Fig. 3 for comparison. The unlabeled spaces (black) surrounded by laminin are filled with unlabeled tumor cells (see Chen et al[7]). Reference bar = 20 μm.

NIH-PA Author Manuscript
NIH-PA Author Manuscript
NIH-PA Author Manuscript

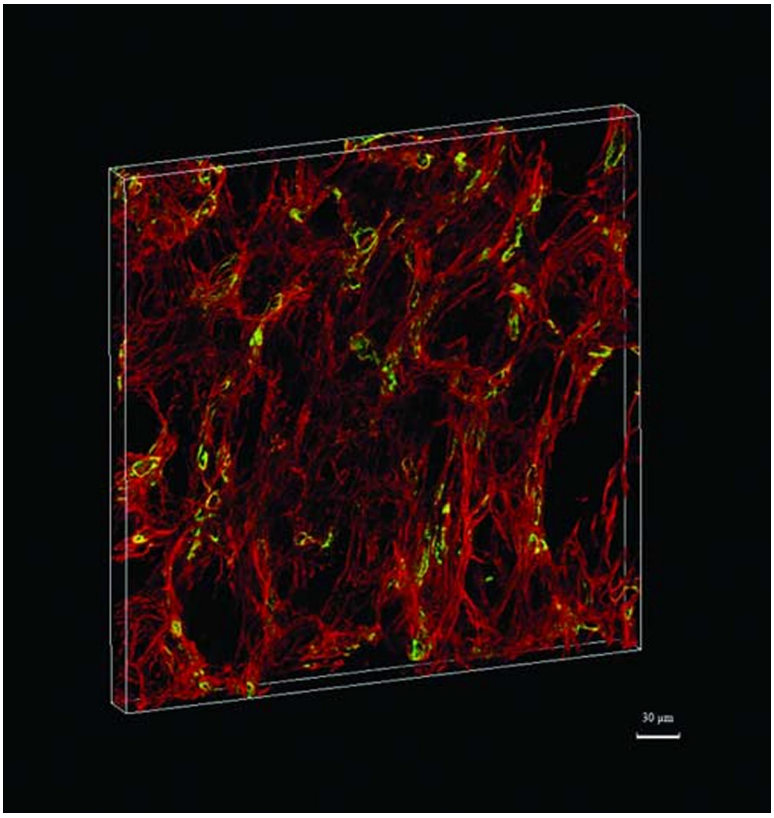

FIGURE 3.

This is a 3D reconstruction of metastatic uveal melanoma to the liver featuring the co-localization of high microvascular density and looping vasculogenic mimicry patterns. The reconstruction includes the area illustrated in Fig. 2 and corresponds to area 4 in Table 1. Laminin is stained red and CD34-positive endothelial cells are stained green. Blood vessels may appear yellow because of the co-localization of laminin and endothelial cells. Resolution of the image is 1.37 × 1.37 × 3.32 pixels/µm measuring 374.78 × 374.78 × 27.39 µm.

NIH-PA Author Manuscript

NIH-PA Author Manuscript

NIH-PA Author Manuscript

Table 1

Microvascular Density Calculations

Area Examined	Area (mm^2) of tissue examined	Number of CD34-positive vessels	Adjusted microvascular density (per 0.313 mm^2 area)	Surface area ratio of laminin-positive VM patterns to CD34-positive vessels
1	0.073	17	72.7	10.9
2	0.101	21	65.0	14.1
3	0.138	25	56.7	10.8
4	0.141	32	71.2	10.8

Calculation of the surface area ratios of laminin-positive VM patterns to CD34-positive vessels was performed based on the area of tissue examined by stitching together overlapping confocal stacks as described in the methods section. Because microvascular density is typically calculated in this tumor system in the literature[20, 36] on the basis of an area of 0.313 mm^2, an adjusted calculation is provided only to allow for a comparison with previously these published data.